

Spatial and temporal dynamics of the crossover from exciton–polariton condensation to photon lasing

This content has been downloaded from IOPscience. Please scroll down to see the full text.

2015 Jpn. J. Appl. Phys. 54 092801

(<http://iopscience.iop.org/1347-4065/54/9/092801>)

View [the table of contents for this issue](#), or go to the [journal homepage](#) for more

Download details:

IP Address: 134.160.214.25

This content was downloaded on 28/09/2015 at 07:01

Please note that [terms and conditions apply](#).

Spatial and temporal dynamics of the crossover from exciton–polariton condensation to photon lasing

Yasuhiro Matsuo^{1,2,3*}, Michael D. Fraser^{2,3}, Kenichiro Kusudo², Andreas Löffler⁴, Sven Höfling⁴, Alfred Forchel⁴, and Yoshihisa Yamamoto^{2,3,5}

¹Graduate School of Information Science and Technology, The University of Tokyo, Bunkyo, Tokyo 113-8656, Japan

²National Institute of Informatics, Chiyoda, Tokyo 101-8403, Japan

³Quantum Functional System Research Group, RIKEN Center for Emergent Matter Science, Wako, Saitama 351-0198, Japan

⁴Technische Physik, Physikalisches Institut, Wilhelm Conrad Röntgen Research Center for Complex Material Systems, Universität Würzburg, 97074 Würzburg, Germany

⁵E. L. Ginzton Laboratory, Stanford University, Stanford, CA 94305, U.S.A.

E-mail: yasuihiro_matsuo@nii.ac.jp

Received March 16, 2015; accepted June 16, 2015; published online August 21, 2015

At a sufficiently high density, the bosonic exciton–polariton system breaks down and the constituent electron, hole, and photon nature is revealed. Although conventional photon lasing is expected in this regime, the nature of the crossover from polariton condensation to photon lasing is not yet well understood. Through detailed mapping, we deconvolute the spatial, temporal, momentum, and energy dependences of the photoluminescence from this system at the crossover point. Photon lasing is distinctly observed far above this crossover.

© 2015 The Japan Society of Applied Physics

1. Introduction

Microcavity exciton polaritons are half-light/half-matter bosonic quasi-particles and can form a Bose–Einstein condensate (BEC) at a sufficiently high phase space density.^{1,2} In 1995, the first observation of a BEC phase was confirmed in a dilute gas of atoms. Experiments with atomic BEC are generally performed in equilibrium, and atomic BEC has been immensely successful as a test bed of fundamental quantum mechanics^{3–7} and condensed matter physics.^{8,9} In contrast, the BEC of exciton–polariton, created in a semiconductor microcavity, is inherently in nonequilibrium owing to the finite polariton lifetime as a result of cavity photon loss. The improving sample quality and emerging techniques for manipulating the polariton condensate render it as an ideal platform for the study of a two-dimensional nonequilibrium quantum degenerate gas.^{10,11}

Unlike the atomic system, polaritons are weakly bound composite particles, and at very high density, they dissociate into predominantly fermionic plasma of electrons and holes coupled to the photon field. It is generally believed that conventional photon lasing, owing to free-carrier population inversion, predominates at high densities, but the nature of the crossover to the high-density phase is presently not well understood. In the experimental literature, this crossover is often referred to as the “2nd threshold” to contrast with the BEC threshold. In this article, through a detailed study of the spatial and temporal dynamics of photoluminescence (PL) from low to high densities, we will investigate the nature of this crossover.

In several theoretical studies, the nature of the microcavity electron–hole high-density regime has been considered. Initially, it was predicted that a standard BEC–BCS crossover would occur in thermal equilibrium,¹² although with substantially different characteristics owing to the interaction of the electron–hole pairs with the photon field.¹³ Subsequent works revealed the origin of the binding force of electron–hole pairs changing from Coulomb to photon-mediated interactions in the high-density regime.^{14,15}

Using a nonequilibrium Greens function approach, recent theoretical works have predicted two different types of 2nd threshold in the high-density regime,^{16,17} one occurring owing to photon lasing under highly nonequilibrium conditions, and the other being a crossover transition into photonic polariton BEC under quasiequilibrium conditions. A notable feature of both scenarios is the existence of an energy gap above that of the free electron–hole pair, implying the existence of bound electron–hole pairs.

In contrast, despite the fact that in experimental studies the 2nd threshold has been widely observed and reported to indicate the onset of photon lasing in a high-excitation regime,^{18–23} there is no clear evidence of either the photonic polariton BEC phase or simple electron–hole bound pairs in the high-density regime.

The standard, simple picture regarding the transition from exciton–polariton condensation to photon lasing is due to the dissociation of Coulomb-bound electron–hole pairs owing to the screening of their binding energy. In the isolated exciton system,²⁴ this transition from insulating exciton gas to electron hole plasma is generally understood to be a gradual transition rather than an abrupt one.^{25,26} Indication of a similarly natured transition in the polariton microcavity system has also recently been indicated by THz spectroscopy.²⁷ The influence of photon interaction via the microcavity is less well understood, but the clear observation of the 2nd threshold and crossover from exciton polariton condensation to photon lasing presents an opportunity to understand the insulator–plasma transition in the microcavity-embedded electron–hole system.

After describing the experimental setup and defining the pump and polarization axes in Sect. 2, we discuss three aspects of the relaxation dynamics of the highly excited microcavity polariton system in Sect. 3. In Sect. 3.1, we consider the time-resolved relaxation dynamics with particular focus on defining the 2nd threshold and characteristic of the crossover from exciton–polariton condensation to photon lasing. In Sect. 3.2, we describe the effect of inhomogeneous and finite- k pumping on the spatial dynamics of the condensate and lasing states. Lastly, in Sect. 3.3 we discuss the

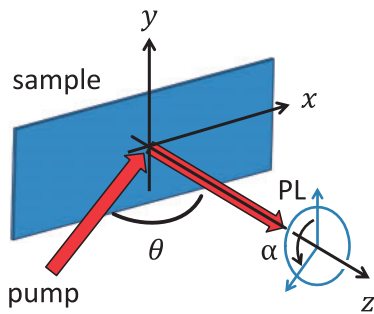


Fig. 1. (Color) Coordinate system of the experimental setup, sample, and pumping geometry. The z -axis is defined to be perpendicular to the sample plane. The pump direction is parallel to the xz -plane and inclined by an angle θ of $\sim 60^\circ$ from the z -axis. The linear polarization angle is characterized by the angle α , where a positive angle indicates a clockwise rotation of the linear polarization vector in the travelling direction of the emitted light. The angle $\alpha = 0^\circ$ is parallel to the y -axis.

temporal polarization dependence and show a linear polarization rotation indicating the cooperative phenomenon of electrons, holes, and photons.

2. Experimental methods

We first define the coordinate system of the experimental setup, sample, and pumping geometry. Figure 1 shows the experimental geometry and definitions of our coordinate nomenclature for the pumping and polarization axes.

Efficient off-resonant photon injection into the microcavity is achieved using a pulsed pump laser at a finite angle (θ of $\sim 60^\circ$) relative to normal incidence, at an energy E_{pump} of ~ 1.668 eV, which couples to the photonic part of the upper polariton branch. The pump source is a mode-locked Ti:sapphire laser with a pulse width of 3 ps and a repetition rate of 76 MHz. At this angled incidence, the pumping spot is focused to an elongated Gaussian with the dimensions $\Delta x \sim 30$ and $\Delta y \sim 20 \mu\text{m}$. The pump polarization is horizontal linear polarization (TM mode).

In order to make the 2nd threshold appear at reasonable laser powers, a sample with a red-detuned cavity mode ($\Delta E = E_{\text{cav}} - E_{\text{exc}}$; ~ -3 meV) is used. The sample structure consists of a $\lambda/2$ cavity with three sets of four 7-nm-wide GaAs/AlAs quantum wells at the antinodes of the cavity mode in a 20- and 16-layer mirror-pair cavity on the bottom and top sides of the microcavity, respectively. A cavity photonic quality factor Q of 2000 is measured. The experiment is conducted at a nominal sample temperature of 10 K.

3. Results and discussion

3.1 BEC–photon lasing crossover

A number of previous works report the observation of the 2nd threshold when increasing the pump power well above the BEC threshold, which is generally described as the crossover from exciton polariton condensation to photon lasing, which is commonly shown in order to substantiate the claim that the 1st threshold characterizes the Bose–Einstein condensation of exciton–polaritons. The 1st and 2nd thresholds are typically defined at the point of a discontinuous change typically in both luminescence intensity and energy at k_{\parallel} of ~ 0 , and in such measurements they are distinguished only by their ordering with increasing pump power.^{1,2,18–20,28}

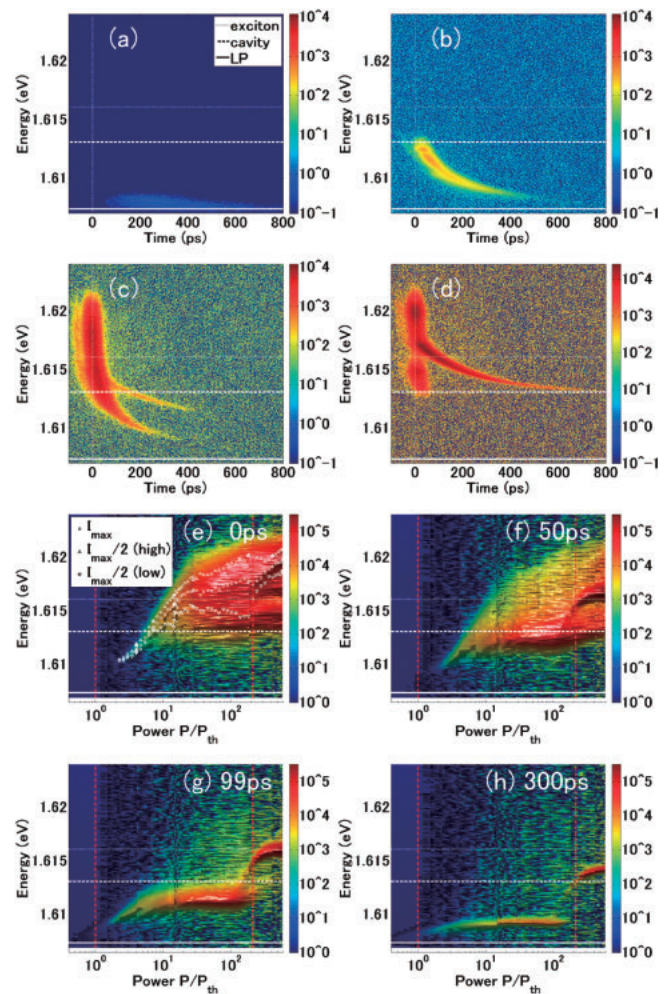


Fig. 2. (Color) (a)–(d) Time-resolved measurement of the emission spectra at k_{\parallel} of ~ 0 . P/P_{th} is (a) 0.7, (b) 5.4, (c) 160, (d) 589. (e)–(h) Pump-power dependence of the emission spectrum at time delays $\Delta t =$ (e) 0, (f) 50, (g) 99, and (h) 300 ps after pumping. Vertical red dotted lines indicate the 1st and 2nd thresholds. 0 ps is defined as the moment the pump emission appears. The exact time delay between pumping and the beginning of photoluminescence at the highest excitation power is a 2–3 ps.

In an inhomogeneously pumped condensate, these characteristics are relatively unambiguous when the pump is Gaussian, and the polariton distribution becomes similarly defined, i.e., with a rough axial symmetry and peaked in a fixed spatial location. However, in the study of the polariton system over the wide range of pump powers studied in this work, it is necessary to carefully deconvolute the energy, momentum, and space dependences. As such, we define the 2nd threshold as in Fig. 2 through the analysis of the time-resolved relaxation spectrum.

Figures 2(a)–2(d) show the time-dependent spectral dynamics of the polariton relaxation following pulsed excitation, for the normalized pump powers P/P_{th} of (a) 0.7, (b) 5.4, (c) 160, and (d) 589. The threshold excitation power density P_{th} is $\sim 1.9 \times 10^{17}$ photons/m²/pulse. The measurement data are taken by isolating the $k_{\parallel} \sim 0$ part of the spectrum using a streak camera and spectrometer slits in the Fourier plane with a time resolution of ~ 2 ps. The experimental data clearly differentiate the different behaviors of (a) a thermal polariton gas below the 1st threshold P_{th} , (b) a polariton BEC above P_{th} , (c) relaxation to both lower

polariton (LP) and cavity photon states immediately below the 2nd threshold, and (d) photon lasing at the cavity photon energy above the 2nd threshold.

Analysis of the PL characteristic as a function of pumping power [Figs. 2(e)–2(h)] at fixed times permits the identification of relaxation dynamics and the intermediate and final states of the system, which are obscured in time-integrated measurements. This measurement results in a clean definition of the 1st and 2nd thresholds. The first occurs at slightly blue-shifted energies above the LP ground state, indicating polariton condensation and the onset of condensate self-interaction. The 2nd threshold is characterized by a coherent emission at the cavity photon energy, indicating the onset of conventional cavity photon lasing.

The pump-power-dependent spectra at fixed time delays Δt of $\sim 0, 50, 99,$ and 300 ps after the initial pump pulse are shown in Figs. 2(e)–2(h), respectively. In each of these figures the two vertical lines indicate the threshold powers for the 1st and 2nd transitions. The cavity photon and single-particle LP energy are also shown as horizontal lines.

Immediately after the pump pulse excites the photoexcited carriers, a wide range of excited states above the cavity photon energy exists [Fig. 2(e)].^{29–32} No distinct LP occupation can be observed at such short timescales. At later times [(f) Δt of ~ 50 ps and (g) Δt of ~ 99 ps], a distinct occupation of the LP and cavity photon states is observed at intermediate and high pumping powers, respectively. However, at such intermediate times, the energy of these states is blue-shifted by the remaining excitons and free-carriers. At (h) Δt of ~ 300 ps, the condensed LP and photon lasing states are clearly developed, and the 2nd transition is clearly visible. As is well established,^{1,2} the 1st transition from thermal polaritons to polariton BEC is exemplified by an abrupt linewidth reduction, a PL intensity increase, and a blue-shift in energy resulting from enhanced bosonic single-mode occupation. The transition from polariton condensation to photon lasing is defined here as the midpoint in the relatively abrupt transition in energy and further linewidth narrowing, where the new energy coincides with that of the cavity photon, at a pump power P of $\sim 213.5P_{th}$. The exact transition power depends sensitively on factors such as sample quality, pump configuration and energy, and cavity-exciton detuning. However, note that it is considerably higher than that of the previous reports of P of $\sim 10P_{th}$.^{18,20,22}

This transition, however, is not abrupt, and between the pump powers P/P_{th} of ~ 100 – 300 , there is a simultaneous occupation in both the LP condensation and photon lasing states before the crossover is complete. With the understanding that, in the electron–hole system, the insulator–plasma transition is also not abrupt, this is not entirely surprising, as it is expected that, over this crossover range of pump powers, the exciton to free-carrier ratio will gradually decrease towards zero. A similarly broad crossover may be observed from the condensate to photon lasing.

Until now, however, we have considered only the low-momentum emission. As the system is inhomogeneously pumped, and at a finite angle corresponding to a finite in-plane angular momentum, we next consider the spatial and momentum dependences of the relaxation dynamics to understand the behavior in the vicinity of $P/P_{th} \sim 200$.

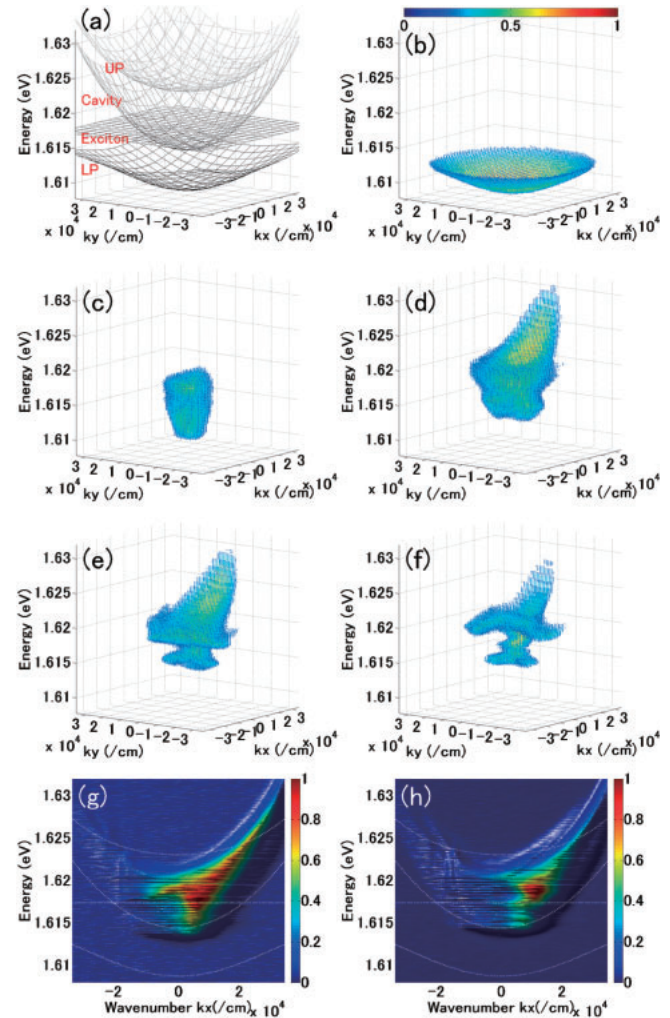


Fig. 3. (Color) (a) Theoretical three-dimensional (3D) dispersion, where the effective mass and ground-state energy are determined by white-light-reflection-spectrum measurement. (b)–(f) Time-integrated 3D dispersion of the photoluminescence at P/P_{th} (b) < 1 , (c) = 40, (d) = 160, (e) = 323, and (f) = 589. We combine k_y -dispersion images measured at each k_x and generate 3D dispersion. The resolution is $\Delta k_y = 0.054 \times 10^4$ /cm and $\Delta k_x = 0.098 \times 10^4$ /cm. (g, h) Cross sections at $k_y = 0$ in (e) and (f).

3.2 Spatial and momentum properties

As the pump angle in a planar microcavity directly controls the initial in-plane momentum of the excited carriers, pumping at a finite angle will induce an asymmetric distribution of momentum and coordinate spatial-resolved relaxation dynamics. Figure 3 shows measurements of the k_x – k_y resolved PL emission at various pump powers. For reference, the theoretical microcavity polariton dispersion for our red-detuned sample (i.e., the LP becomes more photon-like) is schematically shown in Fig. 3(a). The sample parameters are established by a white-light-reflectance measurement of the microcavity.

Figures 3(b)–3(f) show the energy-momentum dispersion of the emission for five pump powers. Figures 3(g) and 3(h) show the cross sections at $k_y = 0$ of Figs. 3(e) and 3(f), respectively. Figure 3(b) shows a clear LP dispersion below the 1st threshold. Figure 3(c) shows the photoemission shift to higher energies and a contraction of momentum space occupation above the threshold for condensation. Figure 3(d) shows the induced carrier emission during the relaxation

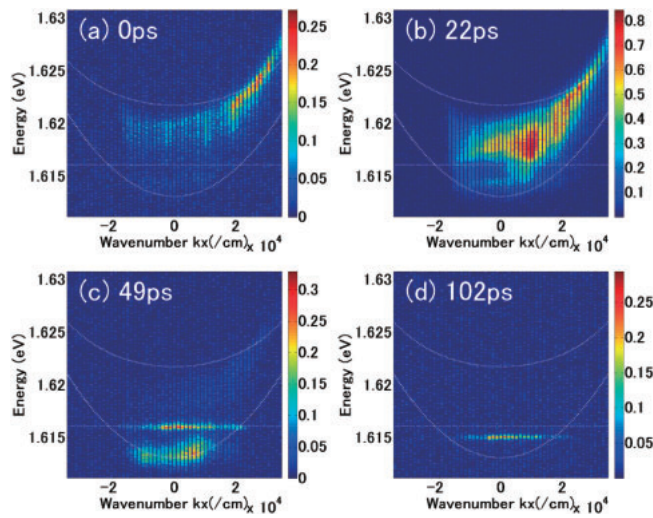


Fig. 4. (Color) Time- and energy-resolved measurement of k_x -dispersion, using a streak camera to measure photoluminescence at each wavenumber. The momentum resolution is $\Delta k_x = 0.128 \times 10^4/\text{cm}$.

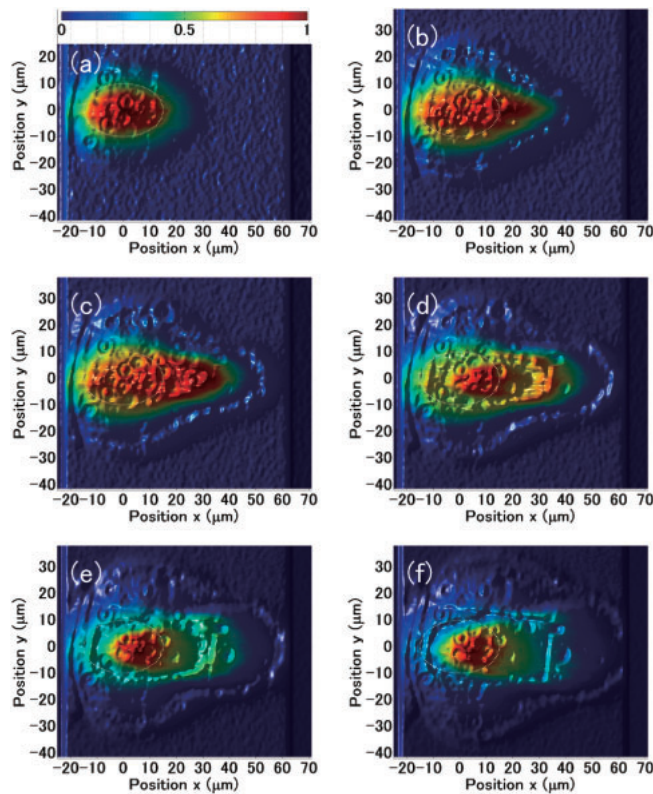


Fig. 5. (Color) Time-integrated and energy-integrated real-space images at $P/P_{\text{th}} =$ (a) 40, (b) 121, (c) 185, (d) 246, (e) 370, and (f) 589.

process in the high-excitation regime, exhibiting an asymmetric emission in the $+k_x$ direction as a result of the finite-angled pump.

In Figs. 3(e)–3(h), when pumping above the 2nd threshold, a peak emission appears at finite momentum. The time-dependent relaxation dynamics of the k_x -asymmetric dispersion in Fig. 3(h) is given in Fig. 4. Figures 4(a) and 4(b) show the emission developing from a blue-shifted cavity mode, evolving into a flat momentum distribution. At a later time, Fig. 4(c) shows that the system shifts to an intermediate stage with the simultaneous occupation of two energy levels,

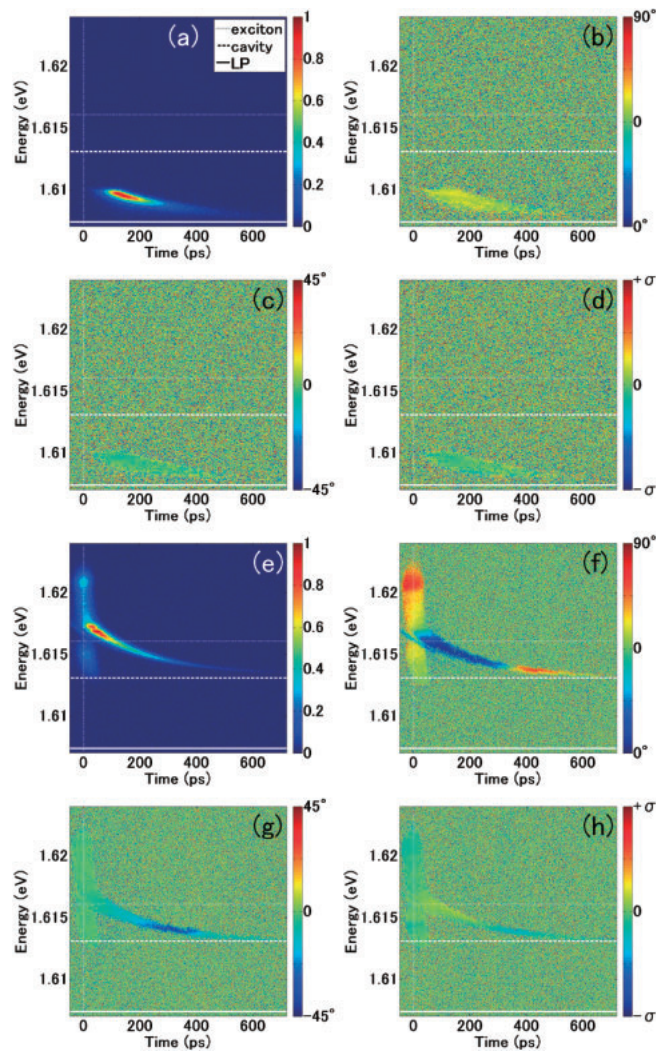


Fig. 6. (Color) Polarization dependence of relaxation spectrum. (a)–(d) Above the 1st threshold. (e)–(h) Above the 2nd threshold. (a, e) Intensity plots. (b, f) S_1 , (c, g) S_2 , and (d, h) S_3 components.

corresponding to the exciton and LP states. 100 ps after pumping, Fig. 4(d) shows that the transition to photon lasing is incomplete.

The effect of finite momentum pumping can also be made clear by analysis of the spatial distribution. For a fixed pump spatial distribution, Fig. 5 shows the time- and energy-integrated spatial distribution as the pumping power is increased. At a low power, but above the BEC threshold [Fig. 5(a)], the (condensate) emission is observed only within the excitation spot. At higher pump powers [Figs. 5(b) and 5(c)], the emission spreads to the $+x$ region. In the high-excitation regime, the in-plane momentum drives the carriers to escape to low-density regions predominantly on the $+x$ side of the pump. It becomes clear that, at the highest pump powers [Figs. 5(d)–5(f)], above the 2nd threshold, the emission concentrates and photon lasing occurs directly within the pump spot.

3.3 Polarization

Our final discussion explores the polarization properties of the PL emission above and below the photon lasing threshold to further clarify the microscopic nature of these states. In Fig. 6, we show the time-dependent polarization dynamics

of the PL emission immediately above the 1st threshold P/P_{th} of ~ 2 [Figs. 6(a)–6(d)] and above the 2nd threshold P/P_{th} of ~ 600 [Figs. 6(e)–6(h)]. For these two laser powers, a full set of energy-time-resolved Stokes parameters,^{33,34} namely, the total intensity $S_0 = I$ [Figs. 6(a) and 6(e)], S_1 [Figs. 6(b) and 6(f)], S_2 [Figs. 6(c) and 6(g)], and S_3 [Figs. 6(d) and 6(h)], are measured, the last three of which are defined as

$$\begin{aligned} S_1 &= \frac{I_{90^\circ} - I_{0^\circ}}{I_{90^\circ} + I_{0^\circ}}, \\ S_2 &= \frac{I_{+45^\circ} - I_{-45^\circ}}{I_{+45^\circ} + I_{-45^\circ}}, \\ S_3 &= \frac{I_{+\sigma} - I_{-\sigma}}{I_{+\sigma} + I_{-\sigma}}. \end{aligned} \quad (1)$$

The linear polarization angle α is defined as the rotation angle about the z -axis as shown schematically in Fig. 1. A positive angle is thus defined as a clockwise rotation in the travelling direction of the emitted light. I indicates the measured intensity of the subscripted polarization component. These measurement data are produced by the cumulative integration of $\sim 76 \times 10^6$ experimental pump pulses, thereby representing the statistical average of polarization of the emitted light.

Above the 1st threshold [Figs. 6(a)–6(d)], each of the Stokes components are close to zero, indicating that the condensate polarization varies shot to shot. The system is pumped at an energy of ~ 60 meV above the LP branch, which is sufficiently energetically separated from the ground state to exhibit strong decay of the polarization information of the pump through multiple phonon and free-carrier scattering events in the relaxation dynamics. Furthermore, the onset of spontaneous coherence via the BEC transition is generally understood to be accompanied by a spontaneous symmetry breaking in the choice of condensate phase and polarization.^{35–37}

In contrast, above the 2nd threshold [Figs. 6(e)–6(h)], the polarization of the high-energy peak initially matches that of the pump pulse. The high pump intensity promotes a more rapid emission of photons from the system, occurring before polarization decoherence becomes significant. As the highly excited system relaxes in energy, the initially pump-driven linear polarization of $\alpha = 90^\circ$ rotates to the linear polarization of 0° over the emission lifetime. The conserved linear polarization and rotation over 500–600 ps implies that a cooperative phenomenon of electrons, holes, and photons is present even in the lasing state.

4. Conclusions

We have reported here an experimental study of the spatial, temporal, and polarization dynamics of the crossover from exciton–polariton condensation to photon lasing. We have revealed new features of this crossover in a spatially inhomogeneously pumped system, in which the spatial coexistence in the relaxation dynamics of the exciton–polariton condensation and the photon lasing above the 2nd threshold are observed. The 2nd threshold P/P_{th} of ~ 213.5 is much higher than the previous P/P_{th} of ~ 10 . The crossover from exciton polariton condensation to photon lasing is clearly identified as a gradual transition rather than an abrupt jump and mimics the typically smooth insulator–plasma transition in an

isolated exciton system. Above the 2nd threshold, the conservation and rotation of linear polarization over 500–600 ps indicate that a cooperative nature of electrons, holes, and photons persists in the lasing state. Although it has been widely accepted that the transition to photon lasing in the microcavity exciton–polariton system is due to the dissociation of electron–hole pairs, our experiments indicate that photon lasing in these structures, particularly near the transition, results from a more complicated interplay of the electron, hole, and photon components of this system and warrants further study.

Acknowledgments

We are grateful to T. Horikiri and M. Yamaguchi for fruitful discussions. This work was funded by the ImPACT Program of Council for Science, Technology and Innovation (Cabinet Office, Government of Japan) and Research for Quantum Repeater Technology (Subject: Entanglement purification between distant nodes), the Commissioned Research of the National Institute of Information and Communications Technology (NICT), Japan.

- 1) H. Deng, G. Weihs, C. Santori, J. Bloch, and Y. Yamamoto, *Science* **298**, 199 (2002).
- 2) J. Kasprzak, M. Richard, S. Kundermann, A. Baas, P. Jeambrun, J. M. J. Keeling, F. M. Marchetti, M. H. Szymańska, R. André, J. L. Staehli, V. Savona, P. B. Littlewood, B. Deveaud, and L. S. Dang, *Nature* **443**, 409 (2006).
- 3) M. H. Anderson, J. R. Ensher, M. R. Matthews, C. E. Wieman, and E. A. Cornell, *Science* **269**, 198 (1995).
- 4) K. B. Davis, M.-O. Mewes, M. R. Andrews, N. J. van Druten, D. S. Durfee, D. M. Kurn, and W. Ketterle, *Phys. Rev. Lett.* **75**, 3969 (1995).
- 5) M. R. Andrews, C. G. Townsend, H.-J. Miesner, D. S. Durfee, D. M. Kurn, and W. Ketterle, *Science* **275**, 637 (1997).
- 6) M. R. Matthews, B. P. Anderson, P. C. Haljan, D. S. Hall, C. E. Wieman, and E. A. Cornell, *Phys. Rev. Lett.* **83**, 2498 (1999).
- 7) J. R. Abo-Shaer, C. Raman, J. M. Vogels, and W. Ketterle, *Science* **292**, 476 (2001).
- 8) M. Greiner, O. Mandel, T. Esslinger, T. W. Hänsch, and I. Bloch, *Nature* **415**, 39 (2002).
- 9) C. A. Regal, M. Greiner, and D. S. Jin, *Phys. Rev. Lett.* **92**, 040403 (2004).
- 10) H. Deng, H. Haug, and Y. Yamamoto, *Rev. Mod. Phys.* **82**, 1489 (2010).
- 11) I. Carusotto and C. Ciuti, *Rev. Mod. Phys.* **85**, 299 (2013).
- 12) J. Keeling, P. R. Eastham, M. H. Szymańska, and P. B. Littlewood, *Phys. Rev. B* **72**, 115320 (2005).
- 13) T. Byrnes, T. Horikiri, N. Ishida, and Y. Yamamoto, *Phys. Rev. Lett.* **105**, 186402 (2010).
- 14) K. Kamide and T. Ogawa, *Phys. Rev. Lett.* **105**, 056401 (2010).
- 15) K. Kamide and T. Ogawa, *Phys. Rev. B* **83**, 165319 (2011).
- 16) M. Yamaguchi, K. Kamide, T. Ogawa, and Y. Yamamoto, *New J. Phys.* **14**, 065001 (2012).
- 17) M. Yamaguchi, K. Kamide, R. Nii, T. Ogawa, and Y. Yamamoto, *Phys. Rev. Lett.* **111**, 026404 (2013).
- 18) J.-S. Tempel, F. Veit, M. Asmann, L. E. Kreilkamp, A. Rahimi-Iman, A. Löffler, S. Höfling, S. Reitzenstein, L. Worschech, A. Forchel, and M. Bayer, *Phys. Rev. B* **85**, 075318 (2012).
- 19) E. Kammann, H. Ohadi, M. Maragkou, A. V. Kavokin, and P. G. Lagoudakis, *New J. Phys.* **14**, 105003 (2012).
- 20) P. Tsotsis, P. S. Eldridge, T. Gao, S. I. Tsintzos, Z. Hatzopoulos, and P. G. Savvidis, *New J. Phys.* **14**, 023060 (2012).
- 21) J. Schmutzler, F. Veit, M. Asmann, J.-S. Tempel, S. Höfling, M. Kamp, A. Forchel, and M. Bayer, *Appl. Phys. Lett.* **102**, 081115 (2013).
- 22) J.-S. Tempel, F. Veit, M. Asmann, L. E. Kreilkamp, S. Höfling, M. Kamp, A. Forchel, and M. Bayer, *New J. Phys.* **14**, 083014 (2012).
- 23) T. Horikiri, Y. Matsuo, Y. Shikano, A. Löffler, S. Höfling, A. Forchel, and Y. Yamamoto, *J. Phys. Soc. Jpn.* **82**, 084709 (2013).
- 24) N. F. Mott, *Rev. Mod. Phys.* **40**, 677 (1968).
- 25) T. Suzuki and R. Shimano, *Phys. Rev. Lett.* **103**, 057401 (2009).
- 26) T. Suzuki and R. Shimano, *Phys. Rev. Lett.* **109**, 046402 (2012).

- 27) J.-M. Ménard, C. Poellmann, M. Porer, U. Leierseder, E. Galopin, A. Lemaître, A. Amo, J. Bloch, and R. Huber, *Nat. Commun.* **5**, 4648 (2014).
- 28) H. Deng, G. Weihs, D. Snoke, J. Bloch, and Y. Yamamoto, *Proc. Natl. Acad. Sci. U.S.A.* **100**, 15318 (2003).
- 29) A. Amo, M. D. Martín, L. Viña, A. I. Toropov, and K. S. Zhuravlev, *Phys. Rev. B* **73**, 035205 (2006).
- 30) L. Kappei, J. Szczytko, F. Morier-Genoud, and B. Deveaud, *Phys. Rev. Lett.* **94**, 147403 (2005).
- 31) S. Chatterjee, C. Ell, S. Mosor, G. Khitrova, H. M. Gibbs, W. Hoyer, M. Kira, S. W. Koch, J. P. Prineas, and H. Stolz, *Phys. Rev. Lett.* **92**, 067402 (2004).
- 32) M. Kira, F. Jahnke, and S. W. Koch, *Phys. Rev. Lett.* **81**, 3263 (1998).
- 33) E. Hecht, *Am. J. Phys.* **38**, 1156 (1970).
- 34) G. Roumpos, C. Lai, T. C. H. Liew, Y. G. Rubo, A. V. Kavokin, and Y. Yamamoto, *Phys. Rev. B* **79**, 195310 (2009).
- 35) H. Ohadi, E. Kammann, T. C. H. Liew, K. G. Lagoudakis, A. V. Kavokin, and P. G. Lagoudakis, *Phys. Rev. Lett.* **109**, 016404 (2012).
- 36) J. J. Baumberg, A. V. Kavokin, S. Christopoulos, A. J. D. Grundy, R. Butté, G. Christmann, D. D. Solnyshkov, G. Malpuech, G. Baldassarri Höger von Högersthal, E. Feltin, J.-F. Carlin, and N. Grandjean, *Phys. Rev. Lett.* **101**, 136409 (2008).
- 37) D. Read, T. C. H. Liew, Yu. G. Rubo, and A. V. Kavokin, *Phys. Rev. B* **80**, 195309 (2009).